ACS MATERIALS Au
AN OPEN ACCESS JOURNAL OF THE AMERICAN CHEMICAL SOCIETY

pubs.acs.org/materialsau
Article

Tunable High Entropy Lanthanide Oxide Microspheres via Confined Electroprecipitation in Emulsion Droplet Scaffolds

Charles H. Laber, Austin R. Scircle, Zachary P. Mouton, Travis Thornell, Ashly Antony, Jonah W. Jurss, and Matthew W. Glasscott*

Cite This: ACS Mater. Au 2024, 4, 179−184
Read Online

ACCESS | Metrics & More | Article Recommendations | Supporting Information

ABSTRACT: Emergent high entropy nanomaterials and their associated complex surface structure hold promise to unlock unique catalytic intermediate pathways and photonic/plasmonic interactions; however, synthetic strategies to tune the size, morphological, and stoichiometric properties remain limited. This work demonstrates a confined electroprecipitation mechanism for the formation of tunable, high-entropy oxide microspheres within emulsion droplet scaffolds. This mechanism complements a traditional confined electrodeposition mechanism and explains the previously observed anomalous formation of thermodynamically unfavorable particles, including lanthanide species. Mass transfer studies reveal that microsphere coverage over a surface may be tuned and modeled by using a time-dependent modified Levich equation. Additionally, morphological tuning was demonstrated as a function of experimental conditions, such as rotation rate and precursor concentration. Finally, extension to multimetallic species permitted the generation of high-entropy lanthanide oxide microspheres, which were confirmed to have equimolar stoichiometries via energy dispersive spectroscopy and inductively coupled plasma mass spectrometry. This novel method promises to generate tunable, complex oxides with applications to thermal catalysis, optics, and applications yet unknown.

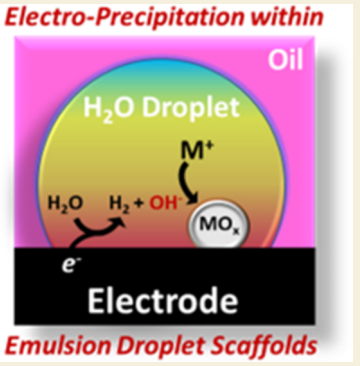

KEYWORDS: *high entropy alloys, high entropy oxides, nanomaterials, lanthanides, electroprecipitation, electrodeposition*

INTRODUCTION

Micromaterials represent an essential enabler of modern technology with applications ranging from electronics[1] and energy conversion[2] to biomedical[3] and environmental sciences.[4] With the consistent demand for advanced materials to forward emerging sustainable, efficient, and cost-effective technologies, novel synthetic strategies which permit tunable control over the size, surface coverage, and stoichiometry of particles are becoming increasingly crucial.[5] Indeed, these properties drive reactivity for various applications including catalysis,[6] plasmonics,[7] and energy storage,[8] and must be rigorously quantified and controlled to both reveal fundamental phenomena and ensure commercial success.

Among common synthetic techniques, electrodeposition of particles onto a surface in situ holds distinct advantages over drop-casting prefabricated particles, chiefly by ensuring an electrical connection is established between the substrate and particle.[9] However, electrodeposition of metal nanoparticles from bulk solutions generally results in heterogeneous particles' sizes, and, in the case of multimetallic particles, stoichiometric heterogeneity.[10] The latter is due to the differing thermodynamic standard reduction potentials between metals, meaning that metals with a lower overpotential for ion reduction will deposit at a greater rate and outcompete less reactive metal precursors. This disadvantage may be overcome by confining metal salts into aqueous droplets suspended in a nonmiscible liquid phase.[11−13] In this experimental scheme, a single droplet collision with an electrode surface produces a nanoparticle with a stoichiometry determined by the droplet contents. Emulsion droplet-mediated electrodeposition has been used to form a variety of materials including monometallic nanoparticles,[14−17] bimetallic nanoparticles,[18] and even high-entropy nanoparticles with up to 8 metal components.[10,19] High entropy materials are either classified (1) numerically by the presence of 5 or more metallic species rendering a calculated entropy > 1.61R, where R is the Universal Gas Constant or (2) empirically through the observation of a crystalline solid-solution microstructural phase stabilized by the elevated mixing entropy.[20] This unique solid-solution microstructural phase is of great interest for enhancing mechanical and catalytic properties.

Within some of these reports, metals not traditionally electrodeposited under aqueous conditions are sometimes incorporated. For instance, lanthanum was alloyed in a $Co_{0.2}Fe_{0.2}La_{0.2}Ni_{0.2}Pt_{0.2}$ particle at a relatively mild deposition

Received: July 26, 2023
Revised: October 17, 2023
Accepted: October 18, 2023
Published: November 6, 2023

potential (−1.3 V vs SHE) despite the fact that the standard reduction potential (E^0) of lanthanum is −2.4 V vs SHE.[10] The difference between the applied potential and formal potential of lanthanum suggests that the reduction reaction will not proceed under these conditions, yet a lanthanum material was observed via elemental analysis. In this work, we explore this thermodynamic discrepancy and show that competitive processes occurring in aqueous droplets at these potentials, namely, the oxygen reduction reaction (ORR) and hydrogen evolution reaction (HER), are responsible for solid lanthanide formation. Since both ORR and HER produce a hydroxide anion as a product, the confined droplet pH may rapidly change and cause oxide precipitates to form spontaneously. The difference between an electrodeposition mechanism and an electroprecipitation mechanism are highlighted in Figure 1.

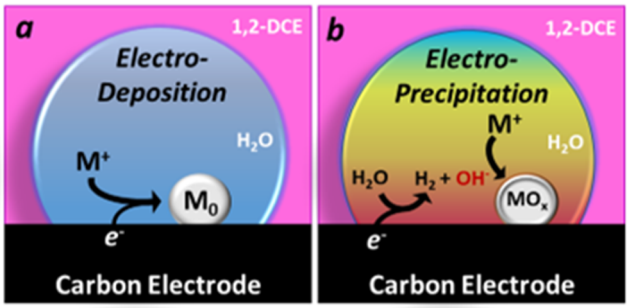

Figure 1. Graphical representation of possible nanoparticle generation in water droplets. (a) Electro-deposition where direct electron transfer to a metal species results in reduction to the metallic zerovalent form and nanoparticle growth. (b) Electro-precipitation mechanism where a sufficient potential is applied to drive water reduction in the droplets, creating a high local pH and resulting in precipitation of a metal ion to an oxidic form.

Figure 1a shows a representative electro-deposition mechanism where a metal ion is reduced at the electrode surface to form a zero valent metal particle,[21] whereas Figure 1b shows an electro-precipitation mechanism where water is reduced at the electrode surface, producing an alkaline gradient which facilitates precipitation of a metal oxide particle.[22,23] We show that this electro-precipitation mechanism generates microspheres that take on the shape of the droplet, effectively meaning the size of the particle may be tuned by altering the average droplet size. Mass transfer studies were also conducted to increase the flux of droplets to the electrode surface, and a modified Levich equation was derived to model the particle coverage. Morphological tuning was demonstrated as a function of experimental conditions, such as rotation rate and precursor concentration. Finally, extension to multi-metallic species permitted the generation of high-entropy oxide microspheres, which were confirmed to have equimolar stoichiometries via energy dispersive spectroscopy (EDS) and inductively coupled plasma mass spectrometry (ICP−MS). This novel method allows the formation of highly tunable, complex oxides, in which the tunability is a valuable feature that promises materials with applications to thermal catalysis, optics, and applications yet unknown.

MATERIALS AND METHODS

Reagents

All chemicals were of analytical grade and used as received. 1,2-Dichloroethane (1,2-DCE, 99.8%) and tetrabutylammonium hexafluorophosphate ($TBAPF_6$, 99%) were obtained from Sigma-Aldrich. Cerium(III) chloride heptahydrate, 99% (cat. no.: A12947); gadolinium(III) chloride hexahydrate, REacton 99.99% (REO) (cat. no.: 011287.06); erbium(III) chloride, anhydrous 99.9% (metals basis) (cat. no.: 089917.09); neodymium(III) chloride hydrate, REacton 99.9% (cat. no.: 011251.18); and terbium(III) chloride hexahydrate, REacton 99.99% (cat. no.: 011210.09) were obtained from Thermo Scientific (Table S1). Stock solutions (1 M) of each metal were prepared in Milli-Q water (>18 MΩ cm) acidified to pH 2 with HCl and diluted as necessary to be used in the emulsion preparation. Metal salt solutions were stored in a dark refrigerator (4 °C) to avoid photodecomposition. Stock solution concentrations were confirmed with ICP−MS and detailed in Table S2. Stock precursor salt concentrations were then added at various ratios to achieve a stoichiometric equivalence in the aqueous phase. No leakage of the lanthanide salts into DCE was observed via UV−vis spectroscopy (Figure S1). Lanthanide metals were present in equimolar concentrations on the surface of the electrode, which was determined via ICP−MS (Table S3).

Instrumentation

The electro-precipitation method was performed using a WaveDriver 200 and WaveVortex (Pine Instruments, Durham, NC) with the chronoamperometry technique (induction at 0 mV for 3 s, step potential at −1.5 V for 300 s, and relaxation at 0 mV for 1 s). The emulsion was prepared using a Q500 ultrasonic processor (Qsonica, Newtown, CT) with a 1/4 in. microtip probe. A Thermo Evolution 350 UV−vis spectrometer (Thermo Fisher Scientific, Waltham, MA) was used to quantify the metal salt leakage from the aqueous emulsion phase to the continuous DCE phase. Scanning electron microscopy (SEM) images and EDX spectra were acquired using a Nanoscience Phenom Pro instrument (Nanoscience, Phoenix, AZ). ICP−MS data were collected using a Nexion 350D (PerkinElmer, Waltham, MA).

Electro-Precipitation Procedure

Oxide microspheres were electro-precipitated on glassy carbon substrate electrodes from a water-in-oil emulsion system previously described in the literature.[14] In summary, a 100 μL aqueous microdroplet containing a total of 1 M lanthanide salt was placed in a 19.9 mL 1,2-DCE continuous phase containing 0.1 M $TBAPF_6$ as a nonaqueous supporting electrolyte and charge balance mediator. An emulsion was produced by sonicating (550 W, amplitude 30%) using a pulse mode method (30 s on, 30 s off, 3 total cycles). Following sonication, a three-electrode electrochemical cell was introduced at a potential sufficient for reducing O_2 and water in the aqueous droplets (−1.5 V vs Ag/AgCl QRE) to facilitate electro-precipitation.

ICP−MS Analysis

Stoichiometric analyses for high coverage HEOx samples were obtained using a PerkinElmer Nexion 350D ICP−MS instrument to supplement EDS analysis for single NPs. Using postdeposition acid washing and ICP−MS to verify surface-bound particle stochiometries has been previously demonstrated as a quantitative compliment to semiquantitative EDS. High coverage samples were prepared by electro-precipitation on a glassy carbon rotating disk electrode (d = 5 mm) at −1.5 V vs Ag/AgCl QRE. Metal stock solutions were prepared for analysis by addition of concentrated nitric acid and diluted to 5% v/v acid matrix in Milli-Q water (>18.2 MΩ cm) prior to ICP−MS analysis. The particles formed on the electrode surface were prepared for metal analysis by submerging and swirling selected electrodes in aqua regia (1:3 HNO_3/HCl, v/v), removal of the electrode, and dilution prior to ICP−MS analysis. The results of the metal stock solutions and the electrode particulate analyses are included in Tables S2 and S3, respectively, of the Supporting Information.

https://doi.org/10.1021/acsmaterialsau.3c00062
ACS Mater. Au 2024, 4, 179−184

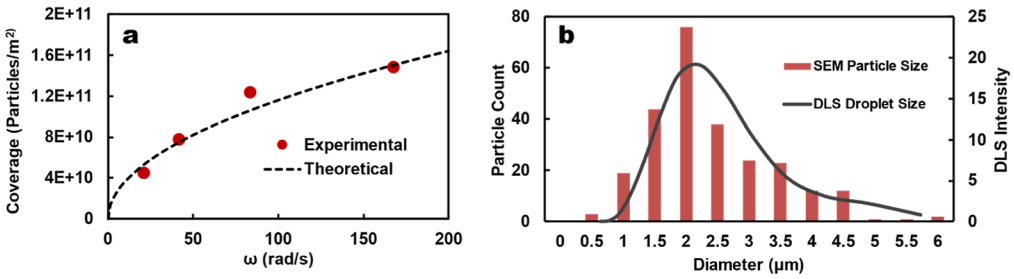

Figure 2. (a) Particle coverage over a glassy carbon macrodisk electrode (r = 2.5 mm) as a function of the angular rotation rate. Experimental data recovered from SEM images postdeposition trends similarly to the theoretical function derived from the Levich equation. Theoretical function assumes $D = 3.4 \times 10^{-13}$ m^2 s^{-1}, $\nu = 6.7 \times 10^{-7}$ m^2 s^{-1}, t = 300 s, and $C^* = 1.2 \times 10^{15}$ droplets·m^{-3}. (b) Particle size distribution histogram from SEM images showing particle size overlaid with droplet size, as measured by dynamic light scattering (DLS). Trend alignment suggests droplet scaffolding for particle deposition.

RESULTS AND DISCUSSION

Enhancing the coverage of particles generated via emulsion droplet deposition proves difficult due to the relatively small diffusion coefficient of microdroplets (on the order of 1×10^{-13} m^2 s^{-1} according to the Stokes−Einstein approximation). A modified Cottrell equation was previously extended to evaluate the predicted nanoparticle coverage on a macro disc electrode, where coverage scales with deposition time and droplet concentration. However, increasing the deposition time frame and droplet concentration can adversely affect emulsion stability;[24] thus, the hypothesis that a rotating disc electrode (RDE) system could be used to quantitatively enhance mass transfer of emulsion droplets to the surface was explored. In order to model the coverage for comparison to the experimental data, a modified Levich equation was derived.

The current to a macro rotating disk electrode may be quantified via the Levich equation[25]

$$i = 0.620nFAD^{2/3}\nu^{-1/6}\omega^{1/2}C^*$$

where n is the number of electrons transferred, F is the Faraday constant, A is the electrode area, D is the diffusion coefficient, ν is the kinematic viscosity, ω is the angular rotation rate, and C^* is the concentration. Recasting the Levich equation for droplet collisions produces the following expression

$$\frac{i}{nF} = \frac{\text{Collisions}}{\text{Second}} = 0.620AD^{2/3}\nu^{-1/6}\omega^{1/2}C^*N_A$$

where D is the diffusion coefficient of the droplets, C^* is the concentration of emulsion droplets, N_A is Avogadro's number, and all other variables are as previously defined. Integrating with respect to time and assuming each droplet collision results in the formation of a single particle[26] permits the calculation of the coverage in particles/m^2

$$\frac{\text{Particles}}{m^2} = 0.620D^{2/3}\nu^{-1/6}\omega^{1/2}C^*N_A t$$

Figure 2a shows this expression plotted against experimental data collected for 300 s on a 2.5 mm radius glassy carbon electrode (Figure S2). The emulsion solution was prepared using 19.9 mL of 1,2-DCE (0.1 M $TBAPF_6$) as the continuous phase with 0.1 mL of aqueous 1 M Ce^{3+} or a lanthanide salt mixture. Assuming an average droplet radius of 1 μm derived from DLS (vide infra), the volume of an individual droplet is approximately 4.2 femtoliters (4.2×10^{-18} m^3). Thus, dividing the total aqueous volume by the volume of an individual droplet and the volume of the continuous phase renders an approximate emulsion concentration of 1.2×10^{15} droplets·m^{-3}. The diffusion coefficient of these droplets may be approximated as 3.4×10^{-13} m^2 s^{-1} using the Stokes−Einstein equation assuming a temperature of 20 °C, a dynamic viscosity of 1,2-DCE of 0.8385 mPa·s,[27] and an average droplet radius of 1 μm. As predicted by the modified Levich expression, the experimental data collected at 200, 400, 800, and 1600 rpm trend with the square root of the angular rotation rate.

It should be noted that previous work deriving mass transfer expressions to carbon electrodes illustrated similar absolute coverage on the order of 10^{11} particles m^{-2} without convective mass transfer stemming from rotation.[26] This apparent discrepancy is due to the order of magnitude difference in droplet concentration previously used ($\sim 1.3 \times 10^{16}$) compared to the lower concentration applied in this study to promote emulsion stability. Thus, these data support the hypothesis that particle coverage on the substrate may be quantitatively enhanced for droplet-mediated deposition by using rotating disk systems.

Examining the particles of the deposits using SEM revealed unique textured spherical morphologies, often with a single circular opening visible. We hypothesized that these morphologies may correlate to the size of the emulsion droplet colliding with the surface, where the small circular area represented the surface contact area, and the spherical particle resulted from a crystallization reaction taking place at the water/1,2-DCE interface. To test this hypothesis, we evaluated the emulsion droplet size distribution by DLS and compared the results to the size distribution for 255 particles rendered from SEM images and processed with ImageJ.[28] Figure 2b reveals the droplet size and particle size data are correlated, supporting the hypothesis that the particles take on the shape of the droplets. These data imply that if the polydispersity of the droplet system can be controlled, the particle size may also be controlled, which will be the subject of a future investigation. Qualitative DLS stability studies and polydispersity information in Figure S4 reveal that the relatively monodisperse (PDI = 0.305) emulsion deteriorates via Ostwalt ripening, forming larger droplets over a period of 1 h.

Due to the highly negative standard reduction potential of Ce^{3+} (−2.4 V vs SHE), it is thermodynamically prohibitive to assume that the particles observed are formed by electroreduction of the cerium cation at −1.5 V vs Ag/AgCl QRE. Based on literature precedent, we expect that cerium oxide particles may be forming due to the reduction of water and oxygen within the emulsion droplets, which would generate hydroxide and thereby precipitate the lanthanide species.[29,30] This deposition mechanism, termed electro-precipitation, was

https://doi.org/10.1021/acsmaterialsau.3c00062
ACS Mater. Au 2024, 4, 179−184

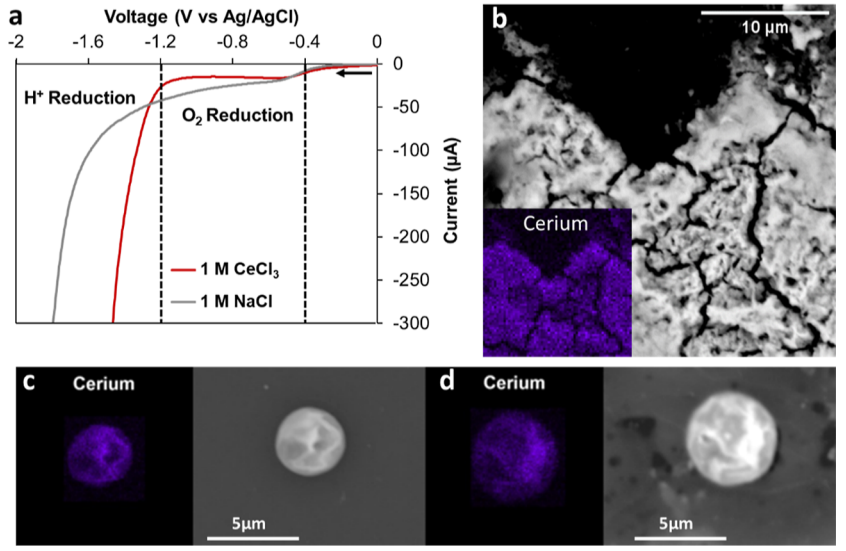

Figure 3. (a) Voltammetry of aqueous 1 M $CeCl_3$ and 1 M NaCl shows regions for electroprecipitation driven by ORR and HER. The working, counter, and reference electrodes were a 2.5 mm radius glassy carbon electrode, a platinum wire, and a Ag/AgCl wire, respectively. (b) SEM of CeO_2 deposits generated via electro-precipitation from a bulk aqueous phase (i.e., with no emulsion present). (c) Cerium particle deposited from 0.1 M Ce^{3+} loading in the droplets; (d) cerium particle 1 M Ce^{3+} loading in the droplets. SEM images in panels C and D indicate that the concentration of lanthanide ion does not change particle morphology or particle size to a significant extent during electro-precipitation.

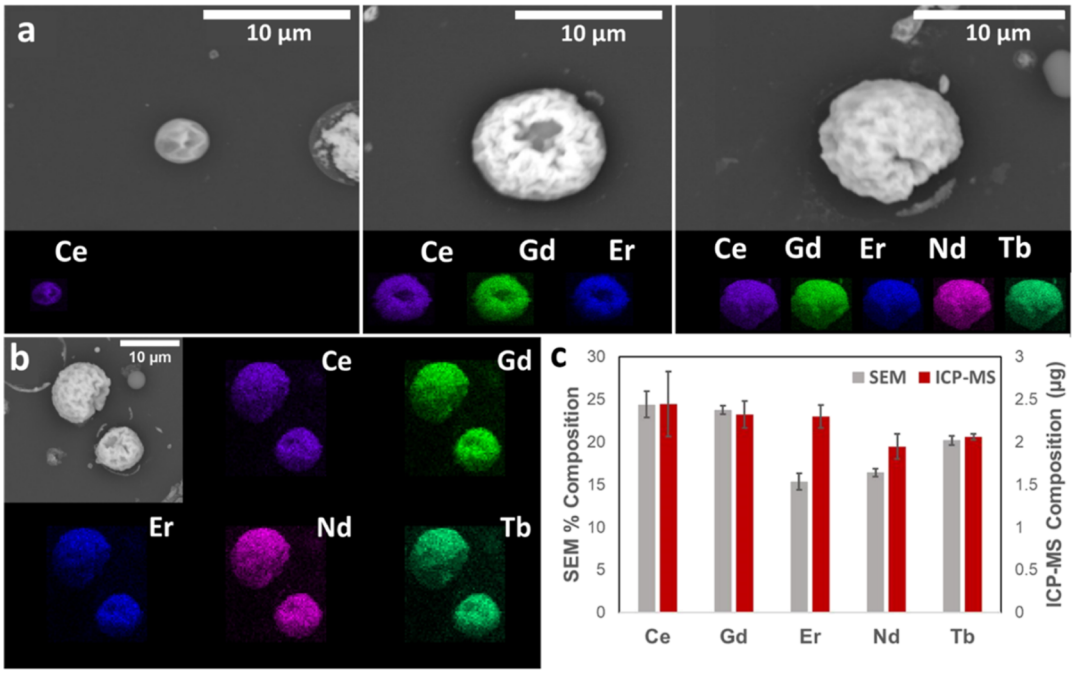

Figure 4. (a) SEM images and EDS maps of HEO_x particles increasing from 1 to 5 lanthanide ions. (b) SEM image and EDS map of multiple HEOx particles with a mixture of 5 lanthanide ions. (c) EDS stoichiometry data of lanthanide ions in particles synthesized from 5 lanthanide ion mixtures compared to the ICP−MS data of particles synthesized from our mixture of 5 lanthanide ions.

explored using voltammetry and correlated SEM Figure 3a shows a voltammogram obtained in 1 M Ce^{3+} and in 1 M NaCl (blank) on a glassy carbon macroelectrode scanned at 100 mV s^{-1}, revealing no electro-reduction until oxygen and water reduction begins at approximately −0.4 and −1.2 V versus Ag/AgCl, respectively. The precipitation of cerium oxide/hydroxide has been observed to catalyze the HER and explains the reduced overpotential and enhanced reaction kinetics compared to the blank voltammogram. Figure 3b shows a SEM image of the electrode surface postvoltammetry in the cerium solution, revealing significant thin-film deposits of CeO_x. This previously observed phenomenon for oxide formation via electroprecipitation also carries into the emulsion droplet system. However, significant control over particle size and morphology is obtained due to the droplet scaffolding effect.

Free proton is consumed rapidly during the initial period of electrolysis

$$2H_3O^+ + 2e^- \rightarrow H_2 + 2H_2O$$

$$O_2 + 4H_3O^+ + 4e^- \rightarrow 6H_2O$$

https://doi.org/10.1021/acsmaterialsau.3c00062
ACS Mater. Au 2024, 4, 179−184

Once proton is quenched, the electro-precipitation process initiates from the release of hydroxide ions during water and oxygen reduction in the neutral/alkaline aqueous phase[31]

$$2H_2O + 2e^- \rightarrow H_2 + 2OH^-$$

$$O_2 + 4e^- + 2H_2O \rightarrow 4OH^-$$

Within this alkaline pH gradient extending from the electrode surface, the cerium cation will undergo an oxidation step by O_2 and a series of hydrolysis steps to form an insoluble cerium oxide.[32] XPS results (Figure S3) confirm the formation of a mixed oxide/hydroxide material composed of $Ce(OH)_3$ and CeO_2.[33]

Figure 3c shows a SEM image of a spherical cerium oxide particle with associated elemental characterization via energy-dispersive X-ray spectroscopy (EDS). The morphology appears to be sphere-like with some surface texturing. While it is not the focus of this study, we hypothesize that the precipitation reaction is occurring selectively at the water/1,2-DCE interface to generate this sphere-like morphology. Multiple factors might be responsible for this phenomenon, including ion transport occurring concomitantly with electron transfer or flux of the oxidant O_2 from the 1,2-DCE phase into the water phase. In order to rule out precursor quenching, experiments at both 0.1 and 1 M Ce^{3+} loading in the droplets were performed, revealing an equivalent structure for similarly sized droplets (Figure 3d). The nature of this interfacial precipitation mechanism will be the subject of future investigation. Due to the polydispersity of the droplet system, particle of different sizes are observed. However, altering the concentration of salt precursor in the droplets did not appear to affect the morphology (i.e., shape).

Due to the confined nature of the precipitation reaction, additional metal salt species may be introduced to the droplets in order to generate complex oxide particles. Figure 4a shows a series of particles deposited from one to five lanthanide metal components. Increasing from one to three lanthanides showed the greatest morphology alterations, with particles primarily forming syncline folds on the surface. The increase from 3 lanthanides to 5 lanthanides resulted in more enclosed particles which can be observed in the far-right panel of Figure 4a. As demonstrated in Figure 4b, this additional lanthanide inclusion is consistently achieved and the oxide particles themselves exhibit a homogeneous incorporation of the lanthanides. Alongside the stoichiometric changes, it appears that the inclusion of these lanthanides subtly alters the morphology of the particles, causing an increased degree of surface striation. Figure 4c shows a semiquantitative EDS measurement compared against a more quantitative ICP–MS analysis of particles over the entire surface. Both data sets reveal a ±5% stoichiometric distribution around the target 20 mol % for each elemental component, indicating a high degree of control and tunability for this electroprecipitation method.

CONCLUSIONS

We have highlighted a distinct method from traditional electro-deposition in water droplets which explains the formation of particles previously suggested to contain zerovalent lanthanide metal species. With the insight provided by the electro-precipitation mechanism in contrast to direct metal ion reduction, these particles are shown to be metal oxide/hydroxides. The presented electro-precipitation strategy permits controlled synthesis of high entropy oxide particles in terms of morphology, particle distribution across the electrode surface, and stoichiometric composition compared with traditional reductive electro-deposition methods, which can lead to inconsistent coatings or stoichiometric imbalance of deposited elements. This electro-precipitation technique presents a wide range of opportunities to enhance the chemical and physical properties by selectively incorporating elements, in desired ratios, into electrode surfaces for enhanced catalytic and other functional properties. Particle coverage may be tuned using a novel time-dependent modified Levich equation. Interestingly, high entropy oxide particles all share a shell like morphology, which may be attributed to a liquid–liquid interfacial precipitation mechanism. This streamlined and accessible strategy for the synthesis of high entropy oxide particles shows promise for a variety of electrocatalytic reactions such as water splitting and applications yet unknown.

ASSOCIATED CONTENT

Supporting Information

The Supporting Information is available free of charge at https://pubs.acs.org/doi/10.1021/acsmaterialsau.3c00062.

Lanthanide salt details, ICP–MS stock concentrations, electrode-bound lanthanide mass, UV–vis leakage experiments, RDE surface coverage data, and DLS emulsion analysis (PDF)

AUTHOR INFORMATION

Corresponding Author

Matthew W. Glasscott − *US Army Engineer Research and Development Center, Environmental Laboratory, Vicksburg, Mississippi 39180, United States;* orcid.org/0000-0001-5743-7738; Email: Matthew.W.Glasscott@usace.army.mil

Authors

Charles H. Laber − *US Army Engineer Research and Development Center, Environmental Laboratory, Vicksburg, Mississippi 39180, United States;* orcid.org/0009-0005-2674-9751

Austin R. Scircle − *US Army Engineer Research and Development Center, Environmental Laboratory, Vicksburg, Mississippi 39180, United States*

Zachary P. Mouton − *US Army Engineer Research and Development Center, Environmental Laboratory, Vicksburg, Mississippi 39180, United States*

Travis Thornell − *US Army Engineer Research and Development Center, Geotechnical and Structures Laboratory, Vicksburg, Mississippi 39180, United States*

Ashly Antony − *The University of Mississippi, Department of Chemistry and Biochemistry, University, Mississippi 38677, United States*

Jonah W. Jurss − *The University of Mississippi, Department of Chemistry and Biochemistry, University, Mississippi 38677, United States;* orcid.org/0000-0002-2780-3415

Complete contact information is available at: https://pubs.acs.org/10.1021/acsmaterialsau.3c00062

Author Contributions

CRediT: **Charles H. Laber** data curation, investigation, methodology, project administration, writing-original draft, writing-review & editing; **Austin R Scircle** data curation, formal analysis, writing-review & editing; **Zachary P Mouton**

https://doi.org/10.1021/acsmaterialsau.3c00062
ACS Mater. Au 2024, 4, 179–184

data curation, formal analysis, methodology; **Travis L. Thornell** data curation; **Ashly Antony** data curation; **Jonah W Jurss** writing-review & editing; **Matthew William Glasscott** conceptualization, funding acquisition, project administration, supervision, visualization, writing-original draft, writing-review & editing.

Notes

The authors declare no competing financial interest.

■ ACKNOWLEDGMENTS

The use of trade, product, or firm names in this report is for descriptive purposes only and does not imply endorsement by the U.S. Government. The tests described and the resulting data presented herein were obtained from research conducted under the US Army Installations and Operational Environments Research & Development Area (US Army Engineer Research and Development Center, ERDC, Project Numbers 493042 and 500994). A.A. and J.W.J. thank the National Science Foundation for funding through CAREER Award CHE-1848478. Permission was granted by the Chief of Engineers to publish this information. The findings of this report are not to be construed as an official Department of the Army position unless so designated by other authorized documents.

■ REFERENCES

(1) Jariwala, D.; Sangwan, V. K.; Lauhon, L. J.; Marks, T. J.; Hersam, M. C. Carbon nanomaterials for electronics, optoelectronics, photovoltaics, and sensing. *Chem. Soc. Rev.* **2013**, *42* (7), 2824−2860.
(2) Arico, A. S.; Bruce, P.; Scrosati, B.; Tarascon, J. M.; Van Schalkwijk, W. Nanostructured materials for advanced energy conversion and storage devices. *Nat. Mater.* **2005**, *4* (5), 366−377.
(3) Lenders, V.; Koutsoumpou, X.; Sargsian, A.; Manshian, B. B. Biomedical nanomaterials for immunological applications: ongoing research and clinical trials. *Nanoscale Adv.* **2020**, *2* (11), 5046−5089.
(4) Luo, J.; Yu, D.; Hristovski, K. D.; Fu, K.; Shen, Y.; Westerhoff, P.; Crittenden, J. C. Critical Review of Advances in Engineering Nanomaterial Adsorbents for Metal Removal and Recovery from Water: Mechanism Identification and Engineering Design. *Environ. Sci. Technol.* **2021**, *55* (8), 4287−4304.
(5) Guardia, P.; Labarta, A.; Batlle, X. Tuning the Size, the Shape, and the Magnetic Properties of Iron Oxide Nanoparticles. *J. Phys. Chem. C* **2011**, *115* (2), 390−396.
(6) Guo, S.; Zhang, S.; Sun, S. Tuning Nanoparticle Catalysis for the Oxygen Reduction Reaction. *Angew. Chem., Int. Ed.* **2013**, *52* (33), 8526−8544.
(7) Li, Z.; Wang, W.; Yin, Y. Colloidal Assembly and Active Tuning of Coupled Plasmonic Nanospheres. *Trends Chem.* **2020**, *2* (7), 593−608.
(8) Augustyn, V. Tuning the interlayer of transition metal oxides for electrochemical energy storage. *J. Mater. Res.* **2017**, *32* (1), 2−15.
(9) Glasscott, M. W.; Pendergast, A. D.; Choudhury, M. H.; Dick, J. E. Advanced Characterization Techniques for Evaluating Porosity, Nanopore Tortuosity, and Electrical Connectivity at the Single-Nanoparticle Level. *ACS Appl. Nano Mater.* **2019**, *2* (2), 819−830.
(10) Glasscott, M. W.; Pendergast, A. D.; Goines, S.; Bishop, A. R.; Hoang, A. T.; Renault, C.; Dick, J. E. Electrosynthesis of high-entropy metallic glass nanoparticles for designer, multi-functional electrocatalysis. *Nat. Commun.* **2019**, *10* (1), 2650.
(11) Glasscott, M. W. *Nanodroplet-Mediated Electrodeposition: Fundamental Principles and Applications to Nanomaterial Synthesis*; The University of North Carolina at Chapel Hill, 2021.
(12) Glasscott, M. W.; Dick, J. E. Electrodeposition in aqueous nanoreactors. *Curr. Opin. Electrochem.* **2021**, *25*, 100637.
(13) Reyes-Morales, J.; Vanderkwaak, B. T.; Dick, J. E. Enabling practical nanoparticle electrodeposition from aqueous nanodroplets. *Nanoscale* **2022**, *14* (7), 2750−2757.
(14) Glasscott, M. W.; Dick, J. E. Fine-Tuning Porosity and Time-Resolved Observation of the Nucleation and Growth of Single Platinum Nanoparticles. *ACS Nano* **2019**, *13* (4), 4572−4581.
(15) Jeun, Y. E.; Baek, B.; Lee, M. W.; Ahn, H. S. Surfactant-free electrochemical synthesis of metallic nanoparticles via stochastic collisions of aqueous nanodroplet reactors. *Chem. Commun.* **2018**, *54* (72), 10052−10055.
(16) Tarolla, N. E.; Voci, S.; Reyes-Morales, J.; Pendergast, A. D.; Dick, J. E. Electrodeposition of ligand-free copper nanoparticles from aqueous nanodroplets. *J. Mater. Chem. A* **2021**, *9* (35), 20048−20057.
(17) Reyes-Morales, J.; Moazeb, M.; Colón-Quintana, G. S.; Dick, J. E. The electrodeposition of gold nanoparticles from aqueous nanodroplets. *Chem. Commun.* **2022**, *58* (76), 10663−10666.
(18) Pendergast, A. D.; Glasscott, M. W.; Renault, C.; Dick, J. E. One-step electrodeposition of ligand-free PdPt alloy nanoparticles from water droplets: Controlling size, coverage, and elemental stoichiometry. *Electrochem. Commun.* **2019**, *98*, 1−5.
(19) Percival, S. J.; Lu, P.; Lowry, D. R.; Nenoff, T. M. Electrodeposition of Complex High Entropy Oxides via Water Droplet Formation and Conversion to Crystalline Alloy Nanoparticles. *Langmuir* **2022**, *38* (5), 1923−1928.
(20) Glasscott, M. W. Classifying and benchmarking high-entropy alloys and associated materials for electrocatalysis: A brief review of best practices. *Curr. Opin. Electrochem.* **2022**, *34*, 100976.
(21) Mohanty, U. S. Electrodeposition: a versatile and inexpensive tool for the synthesis of nanoparticles, nanorods, nanowires, and nanoclusters of metals. *J. Appl. Electrochem.* **2011**, *41* (3), 257−270.
(22) Ramírez-Estrada, A.; Mena-Cervantes, V. Y.; Fuentes-García, J.; Vazquez-Arenas, J.; Palma-Goyes, R.; Flores-Vela, A. I.; Vazquez-Medina, R.; Altamirano, R. H. Cr(III) removal from synthetic and real tanning effluents using an electro-precipitation method. *J. Environ. Chem. Eng.* **2018**, *6* (1), 1219−1225.
(23) Tegladza, I. D.; Xu, Q.; Xu, K.; Lv, G.; Lu, J. Electrocoagulation processes: A general review about role of electro-generated flocs in pollutant removal. *Process Saf. Environ. Prot.* **2021**, *146*, 169−189.
(24) Glasscott, M. W.; Dick, J. E. Direct Electrochemical Observation of Single Platinum Cluster Electrocatalysis on Ultramicroelectrodes. *Anal. Chem.* **2018**, *90* (13), 7804−7808.
(25) Faulkner, A. J. B. a. L. R. *Electrochemical Methods: Fundamentals and Applications*; John Wiley & Sons, 2001.
(26) Glasscott, M. W.; Pendergast, A. D.; Dick, J. E. A Universal Platform for the Electrodeposition of Ligand-Free Metal Nanoparticles from a Water-in-Oil Emulsion System. *ACS Appl. Nano Mater.* **2018**, *1* (10), 5702−5711.
(27) NIST, N. Chemistry WebBook, SRD 69. *Diacetamide* **1988**.
(28) Collins, T. J. ImageJ for microscopy. *Biotechniques* **2007**, *43* (1S), S25−S30.
(29) Świątowska, J.; Lair, V.; Pereira-Nabais, C.; Cote, G.; Marcus, P.; Chagnes, A. XPS, XRD and SEM characterization of a thin ceria layer deposited onto graphite electrode for application in lithium-ion batteries. *Appl. Surf. Sci.* **2011**, *257* (21), 9110−9119.
(30) Majumdar, P.; Gao, R.; White, H. S. Electroprecipitation of Nanometer-Thick Films of Ln(OH)3 [Ln = La, Ce, and Lu] at Pt Microelectrodes and Their Effect on Electron-Transfer Reactions. *Langmuir* **2022**, *38* (26), 8125−8134.
(31) Ge, X.; Sumboja, A.; Wuu, D.; An, T.; Li, B.; Goh, F. W. T.; Hor, T. S. A.; Zong, Y.; Liu, Z. Oxygen Reduction in Alkaline Media: From Mechanisms to Recent Advances of Catalysts. *ACS Catal.* **2015**, *5* (8), 4643−4667.
(32) Scholes, F. H.; Soste, C.; Hughes, A. E.; Hardin, S. G.; Curtis, P. R. The role of hydrogen peroxide in the deposition of cerium-based conversion coatings. *Appl. Surf. Sci.* **2006**, *253* (4), 1770−1780.
(33) Bocchetta, P.; Santamaria, M.; Di Quarto, F. Cerium Oxyhydroxide Nanowire Growth via Electrogeneration of Base in Nonaqueous Electrolytes. *Electrochem. Solid-State Lett.* **2008**, *11* (9), K93.

https://doi.org/10.1021/acsmaterialsau.3c00062
ACS Mater. Au 2024, 4, 179−184